

Computational image analysis of T-cell infiltrates in resectable gastric cancer: association with survival and molecular subtypes

Benjamin R Challoner, BMBS^{1*}, Katharina von Loga, MD^{2,1*}, Andrew Woolston, PhD¹, Beatrice Griffiths, BSc¹, Nanna Sivamanoharan, BSc^{2,1}, Maria Semiannikova, BSc¹, Alice Newey, BSc¹, Louise J Barber, PhD¹, David Mansfield, BSc³, Lindsay C Hewitt, PhD⁴, Yuichi Saito, PhD⁵, Naser Davarzani, PhD,^{4,6} Naureen Starling, MD⁷, Alan Melcher, PhD⁸, Heike I Grabsch, PhD^{4,9#}, Marco Gerlinger, MD^{1,7#}

*these authors contributed equally

#these authors contributed equally

Author affiliations:

¹Translational Oncogenomics Laboratory, Division of Molecular Pathology, The Institute of Cancer Research, 237 Fulham Road, London SW3 6JB, UK

²Translational Immuno-Oncology Team, Centre for Molecular Pathology, The Royal Marsden Hospital NHS Foundation Trust and The Institute of Cancer Research, Cotswold Road, Sutton, SM2 5NG, UK

³Targeted Therapy Team, Division of Radiotherapy and Imaging, The Institute of Cancer Research, 237 Fulham Road, London SW3 6JB, UK

⁴Department of Pathology, Maastricht University Medical Center+, P. Debyelaan 25, 6229 HX Maastricht, Limburg, The Netherlands

⁵Department of Surgery, Teikyo University School of Medicine, 2-11-1 Kaga, Itabashi-ku, Tokyo 173-8605, Japan

⁶Biosystems Data Analysis, Swammerdam Institute for Life Sciences, University of Amsterdam, P.O. Box 94215, 1090 GE, Amsterdam, The Netherlands

⁷Gastrointestinal Cancer Unit, The Royal Marsden Hospital NHS Foundation Trust, Fulham Road, London SW3 6JJ, UK

⁸Translational Immunotherapy Team, Division of Radiotherapy and Imaging, The Institute of Cancer Research, 237 Fulham Road, London SW3 6JB, UK

⁹Pathology & Data Analytics, Leeds Institute of Medical Research at St James's, University of Leeds, St James's University Hospital, Beckett Street, Leeds, LS9 7TF, UK

Corresponding author:

Dr Marco Gerlinger, MD FRCP
Translational Oncogenomics Laboratory
The Institute of Cancer Research, London
237 Fulham Road
London SW3 6JB
United Kingdom
email: marco.gerlinger@icr.ac.uk

ABSTRACT

Background: Gastric and gastro-oesophageal junction cancers (GCs) frequently recur after resection but markers to predict recurrence risk are missing. T-cell infiltrates have been validated as prognostic markers in other cancer types, but not in GC due to methodological limitations of past studies. We aimed to define and validate the prognostic role of major T-cell subtypes in GC by objective computational quantification.

Methods: Surgically resected chemotherapy-naïve GCs were split into discovery (n=327) and validation (n=147) cohorts. CD8 (cytotoxic), CD45RO (memory) and FOXP3 (regulatory) T-cell densities were measured through multicolour immunofluorescence and computational image analysis. Cancer specific survival (CSS) was assessed. All statistical tests were two-sided.

Results: CD45RO-cell and FOXP3-cell densities statistically significantly predicted CSS in both cohorts. Stage, CD45RO-cell and FOXP3-cell densities were independent predictors of CSS in multivariable analysis; mismatch repair (MMR) and Epstein-Barr Virus (EBV) status were not statistically significant. Combining CD45RO-cell and FOXP3-cell densities into the Stomach Cancer Immune Score showed highly statistically significant (all $p \leq 0.002$) CSS differences (0.9y median CSS to not reached). T-cell infiltrates were highest in EBV-positive GCs and similar in MMR-deficient and MMR-proficient GCs.

Conclusion: The validation of CD45RO-cell and FOXP3-cell densities as prognostic markers in GC may guide personalized follow-up or (neo)adjuvant treatment strategies. Only those 20% of GCs with the highest T-cell infiltrates showed particularly good CSS, suggesting that a small subgroup of GCs is highly immunogenic. The potential for T-cell densities to predict immunotherapy responses should be assessed. The association of high FOXP3-cell densities with longer CSS warrants studies into the biology of regulatory T-cells in GC.

Gastric and gastro-oesophageal junction cancers (GCs) are the 3rd commonest cause of cancer-related death worldwide (1). Even localized GCs that are treated aggressively with surgery and peri-operative chemotherapy recur in ~50% of cases (2). Tumour staging is the only prognostic tool in routine clinical use for resectable GCs (3). These tumours are morphologically heterogenous with diffuse- to intestinal-types and well to poorly differentiated phenotypes, but these offer limited prognostic information (4,5). Molecular characterization identified four distinct GC subtypes (6). The most common chromosomally- unstable GCs often harbour driver gene amplifications, followed by genomically-stable GCs with often diffuse-type growth patterns. Microsatellite instable (MSI)/DNA mismatch repair deficient (MMRd) GCs, harbouring high mutation loads, and Epstein-Barr Virus positive (EBV+) GCs are less common and had a better prognosis than chromosomally- unstable and genomically-stable GCs in some series (7).

In colorectal cancer (CRC), tumour-infiltrating lymphocytes have been validated as prognostic markers, independent of stage and MSI-status (8-10). The so-called Immunoscore systematically grades T-cell infiltrates in CRCs which can for example be used to personalize adjuvant treatment or follow-up strategies.

The prognostic relevance of immune cell infiltrates is less clear in GC. Meta-analyses found associations of high cytotoxic- (CD8), helper- (CD4) and memory- (CD45RO) T-cell infiltrates with better survival (11,12). However, the survival differences between high versus low infiltrate GCs were generally modest. The role of regulatory (FOXP3) T-cells, which are considered immunosuppressive, remains unclear with some studies showing an association with longer and others with shorter survival (13).

Immune infiltrates in GC have not been validated as prognostic biomarkers for clinical use due to small cohort sizes in most studies, the use of poorly reproducible manual and semi-quantitative T-cell counting and the lack of validation cohorts (11-13). Moreover, patients in most studies had been treated with a range of different (neo)adjuvant therapies and whether T-cell infiltrates are truly prognostic in early stage GCs or predictive of (neo)adjuvant treatment success remains unknown. Furthermore, studies were predominated by Asian patients whose tumours can differ from Western patients in their immunological profile (14). This questions the relevance to Western populations.

Immunotherapy with PD1/PDL1-inhibitors showed responses in ~10-15% of GCs (15-18). Defining biomarkers that predict who will benefit is critical to avoid unnecessary toxicities and costs. PDL1-positive GCs had higher response rates but PDL1-negative tumours also responded (15), so better predictive biomarkers are a major need. T-cell infiltrates correlated with response to checkpoint-inhibitors in other cancer types (19). Developing computational approaches for the objective quantification of T-cell subtypes in GC and defining their relevance as markers of immunogenicity should not only lead to new prognostic tools but may also support the development of predictive immunotherapy biomarkers.

We used multicolour immunofluorescence staining and computational image analysis to objectively quantify T-cells in 474 GCs resected from Western patients who did not receive (neo)adjuvant therapy. Splitting cases into discovery and validation cohorts allowed us to identify and subsequently validate T-cell subtypes that associate with cancer specific survival (CSS) and finally investigate associations with MMR and EBV molecular subtypes.

MATERIALS AND METHODS:

Patients and samples

The use of archival tissue specimens and of clinico-pathological data for research had been approved by the Leeds Research Ethics Committee (LREC:CA01/122); the need for patient consent was waived by the ethics committee. 0.6mm cores from archival FFPE GCs resected at the Leeds Teaching Hospital between 1985 and 2004 had been embedded into TMAs. EBV and MMR status had been assessed by RNA in-situ hybridisation and immunohistochemistry (20).

Multicolour immunofluorescence staining

Multicolour immunofluorescence staining of one slide per TMA block was performed with the Opal tumor infiltrating lymphocyte kit (PerkinElmer) using CD8, CD4, CD45RO, FOXP3 and pan-cytokeratin antibodies and DAPI (Supplementary table 1).

Computational image analysis

Slides were scanned with a PerkinElmer Vectra using a 20x objective to detect emission at 520/570/670/620/690nm wavelengths (CD4/CD8/CD45RO/FOXP3/pan-cytokeratin, respectively; Supplementary table 2). Signals were unmixed and images exported with PerkinElmer InForm. A pathologist reviewed all 1903 cores to exclude damaged cores and regions with non-malignant epithelium. Cell quantification was performed on TIFF images with the HALO Highplex 3.0 software (Indica Labs). Following fluorescence image acquisition, slides were H&E stained and scanned on a Hamamatsu slide scanner with a 40x objective.

Validation of computational cell quantification

Tissue cores were identified and their surface area quantified with the HALO random forest classifier function. Two pathologists defined thresholds in the HALO software for the computational detection of DAPI stained nuclei, of FOXP3-cells based on Opal620 fluorophore nuclear detection area setting and of CD4-cells, CD8-cells and CD45RO-cells based on cytoplasmic and nuclear detection area settings with Opal520, 570 and 650 fluorophores, respectively (Settings: Supplementary table 3). For validation, a pathologist who was blinded to the computational counts manually annotated all cells stained with a T-cell marker using the HALO annotation function.

The fluorescent FOXP3 staining was also validated against a clinically established chromogenic stain (antigen retrieval in CC1, anti-FOXP3 staining with clone 236A-E7 (eBioscience) at 1:50 dilution) and scanned on a Hamamatsu slide scanner. Cells were quantified using QuPath (21) (Settings: Supplementary table 4).

Statistical analysis

The Spearman rank test was used to measure correlation. CSS was calculated from surgery to GC-related death and analysed with the Kaplan-Meier method and the log-rank test. Follow-up was calculated for patients alive at last follow-up. A Cox regression analysis with stepwise selection was used for multivariable analyses. Statistical test details are provided in the figures. p-values are two-tailed and $p < 0.05$ was considered statistically significant. Statistical tests were performed with R 3.6.1, SPSS 25 or Graphpad Prism.

RESULTS:

Clinical characteristics of the discovery and validation cohorts

FFPE samples from 503 resected GCs from the Leeds Teaching Hospital had been embedded in 14 TMA blocks. Each GC was represented by a minimum of two cores from the area of highest tumour cell density.

This cohort was split approximately 2:1 into a discovery cohort (n=349, the younger tissue samples) and a validation cohort (n=154, older tissue samples). Splitting by tissue age allowed to assess and control for a potential decline of antigenicity over time (22). Patient age, sex and tumour stage were balanced between the cohorts (Table 1). EBV+, MMRd and intestinal type tumours were more common in the validation cohort. This may be due to changes in GC biology over the last decades (23) and random variation when analysing small subgroups. Eight cases who received chemotherapy were excluded, leaving only GCs treated with surgery alone. CSS was available for 327 cases in the discovery cohort (median follow-up 6.6y) and for 147 in the validation cohort (median follow-up 7.3y). These constituted the final analysis groups. CSS was lower in the discovery cohort than in the validation cohort (Supplementary Figure 1). Consistent with recently published data for Western patients (24), survival of MMRd and MMR proficient (MMRp) GC cases was similar (Supplementary Figure 2) and EBV+ cases had a better survival (7). The higher proportion of EBV+ GCs may therefore contribute to the better survival of the validation cohort.

Multicolour immunofluorescence staining

Each cohort was batch stained for CD8 (cytotoxic), CD4 (helper), CD45RO (memory) and FOXP3 (regulatory) T-cells and pan-cytokeratin (epithelial cells) (workflow: Figure 1).

Training and validation of the computational image analysis

Following scanning with an automated microscope, two pathologists defined the threshold settings for computational cell detection. Autofluorescence of elastin fibres and non-specific staining led to high false-positive numbers in the CD4 channel. A threshold for reliable CD4-cell detection could therefore not be defined and these were not included in the analysis. CD8 and CD45RO stains showed specific membranous staining of cells identifiable as lymphocytes on subsequent H&E staining of the same slides. FOXP3 showed dim to intense levels of nuclear staining. All threshold settings were optimised to avoid false positive detection.

For each marker, stained cells were also counted in 20 randomly chosen cores independently by two pathologists. Manual counts from both pathologists showed a high correlation (Spearman $r=0.858-0.968$, all p -values <0.001), demonstrating that the densities of these cells can be reproducibly determined (Figure 2A). A pathologist who was blinded to the computational analysis results subsequently counted cells in 40 cores of each cohort. Comparison with the cell counts from the optimized computational quantification showed a high correlation (Spearman $r=0.845-0.986$, all p -values <0.001 , Figure 2B and C). Computational quantification had a tendency to underestimate cell numbers (apparent in Figures 2B and 2C where data points deviate below the 45 degree line which indicates perfect agreement), particularly when there were few immune cells per core and more pronounced for FOXP3-cells and CD45RO-cells than for CD8-cells. However, the high Spearman correlation coefficient shows that this does not substantially impair the ranking of samples relative to each other. This validated the computational cell quantification.

CD8-cell, CD45RO-cell and FOXP3-cell densities per mm^2 were calculated for each core and the average density across all cores per GC case was used for analysis. All immune

cell types showed higher densities in the discovery cohort compared to the validation cohort (Supplementary Figure 3). This could be a consequence of the higher tissue age in the validation cohort (Table 1) which can impair antigen stability or of batch effects of multicolour immunofluorescence staining.

Correlation of T-cell densities with cancer specific survival in the discovery cohort

The discovery cohort was split into 5 equal-sized groups based on the density of each of the immune cell subtypes (C1-lowest to C5-highest densities). CSS did not statistically significantly differ for CD8-cells ($p=0.08$, Figure 3A), although tumours with the lowest densities (C1) showed a trend towards inferior survival. CD45RO-cell ($p=0.001$) and FOXP3-cell densities ($p<0.001$) were both statistically significantly associated with CSS and showed similar patterns; tumours with the highest densities (C5) had the best survival, those with the lowest densities (C1) had the poorest CSS with a rapid decline over the first 2 years and groups C2-4 showed intermediate survival.

We therefore reclassified groups C2-4 into 60% of cases with intermediate ($CD45RO^{Int}$, $FOXP3^{Int}$), 20% of cases with low ($CD45RO^{Lo}$, $FOXP3^{Lo}$) and 20% of cases with high densities ($CD45RO^{Hi}$, $FOXP3^{Hi}$). These consolidated groups showed highly statistically significant CSS differences ($p<0.001$, Figure 3B) with clinically meaningful differences in median CSS. Examples of immune infiltrates in GCs with low, intermediate and high immune cell densities are shown (Figure 4A).

Validation of the FOXP3 staining

The strong association of higher FOXP3-cell infiltrates with better CSS was surprising as regulatory T-cells are immunosuppressive and predict for a poor prognosis in some

cancer types (25). We therefore validated the fluorescent FOXP3 staining against a clinically established chromogenic FOXP3 stain. Staining of 472 cores from 167 GCs with this assay followed by computational quantification showed a high correlation (Spearman $r=0.830$, $p<0.001$) with fluorescent staining (Figure 4B). Computational cell counts of fluorescent FOXP3 staining were systematically lower than computational counts of the chromogenic stain, revealing systematic biases between the methods. Yet, the high correlation coefficient shows that the ranking of samples remains consistent and validates fluorescent FOXP3-cell quantification.

Validation of the prognostic role of CD45RO- and FOXP3-cell infiltrates

We next assessed whether CD45RO- and FOXP3-cell densities were also prognostic in the validation cohort. Identically to the approach used in the discovery cohort, cases were split into tumours with the highest 20%, intermediate 60% and lowest 20% of immune cell infiltrates. CD45RO-cell and FOXP3-cell densities were also statistically significantly associated with CSS in this cohort ($p=0.02$ and $p=0.003$, respectively, Figure 4C), validating them as prognostic markers in Western GC patients. CSS of the CD45RO^{Lo} and FOXP3^{Lo} groups was less distinct from that of the CD45RO^{Int} and FOXP3^{Int} groups in the validation cohort compared to the discovery cohort. Yet, the rapid decline over the first 2 years remained apparent for CD45RO^{Lo} and FOXP3^{Lo} cases, suggesting that these are important subgroups.

Multivariable analysis

We next investigated whether CD45RO-cells and FOXP3-cells were independent predictors of CSS by analysing them with tumour stage, Lauren classification, EBV and MMR subtypes in a multivariable analysis. CD45RO-cell and FOXP3-cell densities, as well as pT and

pN stage were the only statistically significant predictors of CSS in the discovery and validation cohorts (Table 2 and Supplementary Table 5).

Combining CD45RO- and FOXP3-cell densities into the Stomach Cancer Immune Score

As CD45RO-cell and FOXP3-cell densities were independent prognostic factors, we investigated whether they could be combined to further refine CSS prediction. A 3x3 contingency table defined 9 possible combinations of CD45RO-cell and FOXP3-cell density groups (Figure 5A). The most divergent combinations of CD45RO^{Hi}FOXP3^{Lo} and CD45RO^{Lo}FOXP3^{Hi} comprised very few cases (n=11 and n=2, respectively), which precluded meaningful analysis, and were excluded. CSS was similar for some groups, allowing consolidation into 4 categories, termed the Stomach Cancer Immune Score (STIM-score): CD45RO^{Int}FOXP3^{Lo}, CD45RO^{Lo}FOXP3^{Int} and CD45RO^{Lo}FOXP3^{Lo} were combined into STIM1. CD45RO^{Hi}FOXP3^{Int} and CD45RO^{Int}FOXP3^{Hi} into STIM3. CD45RO^{Hi}FOXP3^{Hi} showed the best CSS and were defined as STIM4 and the largest group of CD45RO^{Int}FOXP3^{Int} tumours was defined as STIM2. Re-analysis by STIM-score was highly statistically significant in the discovery (p<0.001, Figure 5B) and validation cohorts (p=0.002, Figure 5C).

Association of CD45RO- and FOXP3-cell densities with molecular characteristics

MMRd and EBV+ GCs are considered particularly immunogenic due to high mutation burdens and virus presence, respectively. We therefore assessed how immune cell densities differed between these subtypes. 87.5% and 50.0% of EBV+ tumours from the discovery and the validation cohort, respectively, were STIM3 or STIM4 (Figure 5B-C), supporting higher immune recognition of EBV+ compared to MMRp/EBV- GCs of which only 30.9% in the discovery cohort and 26.2% in the validation cohort were STIM3/STIM4. The percentage of

GCs that were classed as STIM3/STIM4 was similar for MMRd GCs and MMRp/EBV- GCs (Figure 5B and C).

Comparing immune cell densities directly between molecular subgroups showed that CD45RO-cell densities were statistically significantly higher in EBV+ than in MMRp/EBV- GCs in the discovery and the validation cohorts (Figure 6A-B). FOXP3-cell densities were statistically significantly higher in EBV+ GCs compared to MMRp/EBV- tumours in the discovery cohort (Figure 6A) but not in the validation cohort (Figure 6B). MMRd GCs only showed a higher density of CD45RO-cells compared to MMRp/EBV- GCs in the discovery cohort (Figure 6A). The small number of EBV+ and MMRd cases may have contributed to these differences between discovery and validation cohorts.

DISCUSSION:

Multicolour immunofluorescence coupled with computational image analysis identified and validated CD45RO-cell and FOXP3-cell densities as prognostic markers in Western GC patients, independent of stage, MMR and EBV status and other pathological features. Those 20% of patients with the highest densities of CD45RO-cells and of FOXP3-cells had a particularly good CSS whereas the three groups with intermediate densities showed similar CSS. GCs with the lowest densities showed a rapid early decline in CSS. Most previous GC studies defined high and low T-cell infiltrate groups based on a median cut-off value (11-13), which may explain the weak prognostic effect they found for immune infiltrates compared to the large differences shown by our analysis.

Our results provide important insights into GC immunobiology, suggesting that immunogenicity is low or that immunosuppressive factors constrain immune recognition in the majority of tumours, so that only 20% of cases achieve major survival benefits from T-cell infiltration. CD45RO-cells are considered long-lived memory T-cells which are generated in response to cognate antigen recognition (10). Abundant CD45RO-cells may hence identify GCs that have been actively detected by T-cells. In contrast, CD8-cells were not statistically significantly associated with CSS, perhaps indicating that a large proportion of these are passive bystanders that do not recognize cancer cells (26). FOXP3 is a marker for regulatory T-cells described as immunosuppressive. The paradoxical association of a cell type that is thought to inhibit anti-tumour immunity with a good prognosis may point to the existence of distinct subtypes of suppressive and non-suppressive regulatory T-cells, as recently described in CRCs (27). Furthermore, *in vitro* experiments reported FOXP3 expression as an early activation marker in T-cells without suppressive function (28). Our results warrant further investigation of the biology of FOXP3-cells in GC and suggests caution when applying immunotherapies that inhibit or deplete regulatory T-cells in GCs.

With response rates for PD1/PDL1-inhibitors of 10-15% (16-18), immunotherapy sensitivity is also confined to a small subgroup of GCs. In addition, PD1/PDL1-inhibitors are predominantly effective against tumours that are spontaneously recognized by the immune system which manifests in higher T-cell infiltrates and IFN-gamma signatures, among others (29). Investigating whether high CD45RO-cell or FOXP3-cell infiltrates can identify GCs with high spontaneous immunogenicity that will also respond to immunotherapy will be an important next step, particularly as PDL1 expression is a poor predictive biomarker for checkpoint-inhibitors in GC (18,30). Understanding the molecular basis that results in low

immune cell infiltrates in 20% of cases with the associated rapid survival decline may lead to novel therapeutic opportunities for this group of patients.

Our data furthermore revealed high CD45RO-cell and FOXP3-cell infiltrates in EBV+ GCs. Surprisingly, T-cell densities in MMRd GCs were similar to MMRp/EBV- GCs. We recently showed that the hypermutator phenotype in MMRd GCs confers extreme intratumour heterogeneity that enables the evolution of multiple genetic immune-evasion events within individual tumours (31). This ability to readily acquire mutations in immune-evasion regulators, and potentially the activity of non-genetic immune escape mechanisms such as high beta-Catenin activity (32) or mesenchymal features (33), may perhaps explain low immune infiltrates in many MMRd GCs.

This large study in GC patients who had been treated with surgery alone defines T-cell subtypes that influence the natural history of GCs. This unique cohort can be used as a comparator when assessing the predictive role of immune cells in GC immunotherapy trials that do not include an untreated control group. Comparison to GCs treated with peri-operative or adjuvant chemotherapy should be undertaken to further define the predictive role of T-cell infiltrates for chemotherapy outcomes.

We finally devised a strategy combining both cell types into the 'STIM-score' which is more straightforward to apply in the clinic than two separate markers and identifies patient groups with clinically meaningful differences in CSS. This could be useful to identify patients with low recurrence risks who may not require intensive adjuvant or peri-operative chemo/chemoradiotherapy or to prioritize those patients with very poor survival outcomes for treatment intensification trials.

Before the STIM-score can be clinically applied, optimal T-cell density cut-offs should be defined in diagnostic GC biopsies and in resected GCs whole slides as these may differ

from cut-offs determined in TMAs. Limitations of this study include a lack of CD4-cell analysis, the specimen age of up to 33 years, and the absence of samples from tumour margins in the TMA which precluded investigating tumour margins and centres similar to the Immunoscore approach (8-10). Finally, independent validation in GC cohorts from additional centres should be undertaken.

FUNDING

MG receives funding from Cancer Research UK, the Schottlander Foundation and from the European Research Council (ERC) under the European Union's Horizon 2020 research and innovation programme (grant agreement No. 820137). MG, BC, NSt and KvL receive funding from the Royal Marsden Hospital/ICR NIHR Biomedical Research Centre for Cancer.

NOTES

Role of the funder: The funders had no role in the design of the study; the collection, analysis, and interpretation of the data; the writing of the manuscript; and the decision to submit the manuscript for publication

Competing interests: MG receives research funding from Merck KG and BMS, NSt from BMS, Astra Zeneca, Pfizer, Merck KG and honoraria from Eli-Lilly, Astra Zeneca, MSD, Merck KG and Pierre Fabre.

Author contributions: MG, HG and KvL planned the study. KvL and MG obtained funding. MG led the study. HG provided clinical samples, data and statistical expertise. LH and YS were involved in data collection. BC, KvL, NSi and DM optimized and performed staining, scanning and computational image analysis and BG provided technical support. BC analysed all data with help from HG, KvL, LB, MS, AN and AW. BC, KvL, ND, NSt, AM, HG and MG interpreted the data. All authors were involved in manuscript writing and gave final approval of the manuscript.

REFERENCES

1. Bray F, Ferlay J, Soerjomataram I, *et al.* Global cancer statistics 2018: GLOBOCAN estimates of incidence and mortality worldwide for 36 cancers in 185 countries. *CA Cancer J Clin* 2018;68(6):394-424.
2. Al-Batran SE, Homann N, Pauligk C, *et al.* Perioperative chemotherapy with fluorouracil plus leucovorin, oxaliplatin, and docetaxel versus fluorouracil or capecitabine plus cisplatin and epirubicin for locally advanced, resectable gastric or gastro-oesophageal junction adenocarcinoma (FLOT4): a randomised, phase 2/3 trial. *Lancet* 2019;393(10184):1948-1957.
3. Brierley Je, Gospodarowicz MKe, Wittekind Ce. *TNM classification of malignant tumours*. Eighth edition. ed.
4. Gullo I, Oliveira P, Athelougou M, *et al.* New insights into the inflamed tumor immune microenvironment of gastric cancer with lymphoid stroma: from morphology and digital analysis to gene expression. *Gastric Cancer* 2019;22(1):77-90.
5. Lee JH, Chang KK, Yoon C, *et al.* Lauren Histologic Type Is the Most Important Factor Associated With Pattern of Recurrence Following Resection of Gastric Adenocarcinoma. *Ann Surg* 2018;267(1):105-113.
6. Cancer Genome Atlas Research N. Comprehensive molecular characterization of gastric adenocarcinoma. *Nature* 2014;513(7517):202-9.
7. Cristescu R, Lee J, Nebozhyn M, *et al.* Molecular analysis of gastric cancer identifies subtypes associated with distinct clinical outcomes. *Nat Med* 2015;21(5):449-56.
8. Anitei MG, Zeitoun G, Mlecnik B, *et al.* Prognostic and predictive values of the immunoscore in patients with rectal cancer. *Clin Cancer Res* 2014;20(7):1891-9.
9. Galon J, Costes A, Sanchez-Cabo F, *et al.* Type, density, and location of immune cells within human colorectal tumors predict clinical outcome. *Science* 2006;313(5795):1960-4.
10. Galon J, Pages F, Marincola FM, *et al.* The immune score as a new possible approach for the classification of cancer. *J Transl Med* 2012;10:1.
11. Yu PC, Long D, Liao CC, *et al.* Association between density of tumor-infiltrating lymphocytes and prognoses of patients with gastric cancer. *Medicine (Baltimore)* 2018;97(27):e11387.
12. Zheng X, Song X, Shao Y, *et al.* Prognostic role of tumor-infiltrating lymphocytes in gastric cancer: a meta-analysis. *Oncotarget* 2017;8(34):57386-57398.
13. Huang Y, Liao H, Zhang Y, *et al.* Prognostic value of tumor-infiltrating FoxP3+ T cells in gastrointestinal cancers: a meta analysis. *PLoS One* 2014;9(5):e94376.

14. Lin SJ, Gagnon-Bartsch JA, Tan IB, *et al.* Signatures of tumour immunity distinguish Asian and non-Asian gastric adenocarcinomas. *Gut* 2015;64(11):1721-31.
15. Fuchs CS, Doi T, Jang RW, *et al.* Safety and Efficacy of Pembrolizumab Monotherapy in Patients With Previously Treated Advanced Gastric and Gastroesophageal Junction Cancer: Phase 2 Clinical KEYNOTE-059 Trial. *JAMA Oncol* 2018;4(5):e180013.
16. Kang YK, Boku N, Satoh T, *et al.* Nivolumab in patients with advanced gastric or gastro-oesophageal junction cancer refractory to, or intolerant of, at least two previous chemotherapy regimens (ONO-4538-12, ATTRACTION-2): a randomised, double-blind, placebo-controlled, phase 3 trial. *Lancet* 2017;390(10111):2461-2471.
17. Muro K, Chung HC, Shankaran V, *et al.* Pembrolizumab for patients with PD-L1-positive advanced gastric cancer (KEYNOTE-012): a multicentre, open-label, phase 1b trial. *Lancet Oncol* 2016;17(6):717-726.
18. Wang F, Wei XL, Wang FH, *et al.* Safety, efficacy and tumor mutational burden as a biomarker of overall survival benefit in chemo-refractory gastric cancer treated with toripalimab, a PD-1 antibody in phase Ib/II clinical trial NCT02915432. *Ann Oncol* 2019;30(9):1479-1486.
19. Tumei PC, Harview CL, Yearley JH, *et al.* PD-1 blockade induces responses by inhibiting adaptive immune resistance. *Nature* 2014;515(7528):568-71.
20. Hewitt LC, Inam IZ, Saito Y, *et al.* Epstein-Barr virus and mismatch repair deficiency status differ between oesophageal and gastric cancer: A large multi-centre study. *Eur J Cancer* 2018;94:104-114.
21. Bankhead P, Loughrey MB, Fernandez JA, *et al.* QuPath: Open source software for digital pathology image analysis. *Sci Rep* 2017;7(1):16878.
22. Combs SE, Han G, Mani N, *et al.* Loss of antigenicity with tissue age in breast cancer. *Lab Invest* 2016;96(3):264-9.
23. Arnold M, Park JY, Camargo MC, *et al.* Is gastric cancer becoming a rare disease? A global assessment of predicted incidence trends to 2035. *Gut* 2020; 10.1136/gutjnl-2019-320234.
24. Pietrantonio F, Miceli R, Raimondi A, *et al.* Individual Patient Data Meta-Analysis of the Value of Microsatellite Instability As a Biomarker in Gastric Cancer. *J Clin Oncol* 2019;37(35):3392-3400.
25. deLeeuw RJ, Kost SE, Kakal JA, *et al.* The prognostic value of FoxP3+ tumor-infiltrating lymphocytes in cancer: a critical review of the literature. *Clin Cancer Res* 2012;18(11):3022-9.
26. Simoni Y, Becht E, Fehlings M, *et al.* Bystander CD8(+) T cells are abundant and phenotypically distinct in human tumour infiltrates. *Nature* 2018;557(7706):575-579.
27. Saito T, Nishikawa H, Wada H, *et al.* Two FOXP3(+)CD4(+) T cell subpopulations distinctly control the prognosis of colorectal cancers. *Nat Med* 2016;22(6):679-84.

28. Kmiecik M, Gowda M, Graham L, *et al.* Human T cells express CD25 and Foxp3 upon activation and exhibit effector/memory phenotypes without any regulatory/suppressor function. *J Transl Med* 2009;7:89.
29. Trujillo JA, Sweis RF, Bao R, *et al.* T Cell-Inflamed versus Non-T Cell-Inflamed Tumors: A Conceptual Framework for Cancer Immunotherapy Drug Development and Combination Therapy Selection. *Cancer Immunol Res* 2018;6(9):990-1000.
30. Kelly RJ. Immunotherapy for Esophageal and Gastric Cancer. *Am Soc Clin Oncol Educ Book* 2017;37:292-300.
31. von Loga K, Woolston A, Punta M, *et al.* Extreme intratumour heterogeneity and driver evolution in mismatch repair deficient gastro-oesophageal cancer. *Nat Commun* 2020;11(1):139.
32. Luke JJ, Bao R, Sweis RF, *et al.* WNT/beta-catenin Pathway Activation Correlates with Immune Exclusion across Human Cancers. *Clin Cancer Res* 2019;25(10):3074-3083.
33. Kim ST, Cristescu R, Bass AJ, *et al.* Comprehensive molecular characterization of clinical responses to PD-1 inhibition in metastatic gastric cancer. *Nat Med* 2018;24(9):1449-1458.

TABLES

Table 1 Clinical and pathological characteristics of the discovery and validation cohorts

Variables	Discovery cohort (n= 341)	Validation cohort (n=154)	p-value*
Median year of resection	1997	1992	
Median age (range)	72.0 y (29.4-90.0)	70.5 y (33.8-90.5)	0.30
Sex			
Male	63.3% (216)	66.2% (102)	
Female	36.1% (123)	33.8 % (52)	0.59
pT (UICC TNM 7th edition)			
pT1	8.8% (30)	5.8% (9)	
pT2	7.9% (27)	10.4% (16)	
pT3	28.4% (97)	36.4% (56)	
pT4	54.8% (187)	47.4% (73)	0.30
pN (UICC TNM 7th edition)			
pN0	25.9% (88)	25.3% (39)	
pN1 to pN3b	74.1% (252)	74.7% (115)	0.79
pM (UICC TNM 7th edition)			
pM0/Mx	97.4% (332)	95.5% (147)	
pM1	2.6% (9)	4.5% (7)	0.40
Stage (UICC TNM 7th edition)			
I	12.6% (43)	9.1 (14)	
II	24.4% (83)	28.6 (44)	
III	60.3% (205)	57.8 (89)	
IV	2.6% (9)	4.5% (7)	0.69
Lauren classification			
Intestinal	56.0% (191)	75.2% (115)	
Diffuse	27.3% (93)	13.7% (21)	
Mixed	16.4% (56)	11.1% (17)	<0.001
MMR status			
Proficient	91.7% (299)	84.4% (130)	
Deficient	8.3% (27)	15.6% (24)	0.02
No MMR data available	4.3% (15)	0.0% (0)	
EBV status			
Negative	97.5% (306)	92.2% (141)	
Positive	2.5% (8)	7.8% (12)	0.02
No EBV data available	7.7% (27)	0.6% (1)	

*Two-sided, Chi-Squared tests.

Table 2 – Final statistically significant variables of the multivariable Cox regression analysis of the discovery cohort and assessment of these in the validation cohort.

Variable	Discovery cohort		Validation cohort	
	Hazard ratio (95% CI)	p-value*	Hazard ratio (95% CI)	p-value*
CD45RO cell density				
Hi	1.00 (Reference)	-	1.00 (Reference)	-
Int	1.71 (1.11 to 2.65)	0.02	1.59 (0.74 to 3.44)	0.24
Lo	2.09 (1.25 to 3.48)	0.005	2.59 (1.09 to 6.18)	0.03
FOXP3 cell density				
Hi	1.00 (Reference)	-	1.00 (Reference)	-
Int	2.00 (1.21 to 3.29)	0.007	3.19 (1.25 to 8.15)	0.02
Lo	2.79 (1.54 to 5.08)	0.001	3.28 (1.19 to 9.06)	0.02
Stage (UICC TNM 7 th Edition)				
pT3/4	1.00 (Reference)	-	1.00 (Reference)	-
pT1/2	0.22 (0.10 to 0.45)	<0.001	0.29 (0.10 to 0.80)	0.02
pN1-3	1.00 (Reference)	-	1.00 (Reference)	-
pN0	0.45 (0.29 to 0.70)	<0.001	0.37 (0.18 to 0.74)	0.005

*Two-sided, Cox regression analysis.

FIGURE LEGENDS

Figure 1 Immune staining and computational analysis workflow.

Figure 2 Correlation of pathologist and computational immune cell quantification. (A) Correlation of CD8-cells, CD45RO-cells and FOXP3-cells counted independently by two pathologists (n=20 cores). (B) Correlation of computational quantification with counts by a pathologist in the discovery cohort (n=40). (C) Correlation of computational quantification with counts by a pathologist in the validation cohort (n=40). The grey 45° line indicates where identical counts lie; where computational counts were greater than manual counts the data points are above the line and where computational counts were lower than manual counts the data points are below. The Spearman correlation coefficient and p-values are shown. All tests were two-sided.

Figure 3 Kaplan-Meier analysis of cancer specific survival by CD8-cell, CD45RO-cell and FOXP3-cell density in the discovery cohort. (A) Cancer specific survival for each of the 5 equal-sized groups. (B) Cancer specific survival for the 3 density groups. Dashed lines indicate the median survival time for individual groups. p-values were calculated with a log-rank test. All tests were two-sided.

Figure 4 Multi-modal data validation. (A) Representative multicolour fluorescence images of TMA cores with high (Hi), intermediate (Int) and low (Lo) density infiltrates of CD8-cells

(green), CD45RO-cells (red), FOXP3-cells (yellow). All scale bars = 50 μ m. (B) Correlation of computationally counted FOXP3-cells stained with chromogenic vs fluorescent immunohistochemistry from 167 patients. The grey 45° line indicates where identical counts lie. The Spearman correlation coefficient and p-values are shown. (C) Kaplan Meier analysis of cancer specific survival by CD45RO-cell and FOXP3-cell density in the validation cohort. Dashed lines indicate the median survival time for individual groups. p-values were calculated with a log-rank test. All tests were two-sided.

Figure 5 Combination of CD45RO-cell and FOXP3-cell densities into the Stomach Cancer Immune-Score (STIM-score). (A) A 3x3 contingency table of CD45RO-cell and FOXP3-cell density classes. A Kaplan-Meier analysis of the 7 colour coded groups is shown on the right. (B) Kaplan-Meier analysis of the consolidated STIM-score in the discovery cohort and (C) the validation cohort. Dashed lines indicate the median survival time for individual groups. The data table shows the distribution of EBV+, MMRd and MMRp/EBV- cases according to STIM-score. p-values were calculated with a log-rank test. All tests were two-sided.

Figure 6 Association of CD45RO-cell and FOXP3-cell densities with MMR and EBV status in (A) the discovery cohort and (B) the validation cohort. Densities were off-set by 1 before log transformation. Red bars indicate the mean and p-values were calculated with unpaired t-tests on non-transformed data. All tests were two-sided.

Figure 1

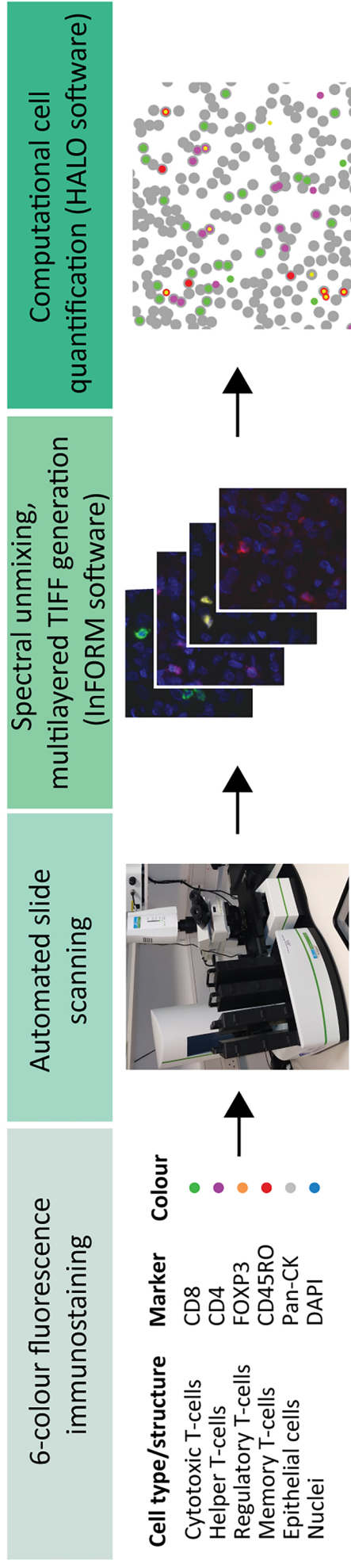
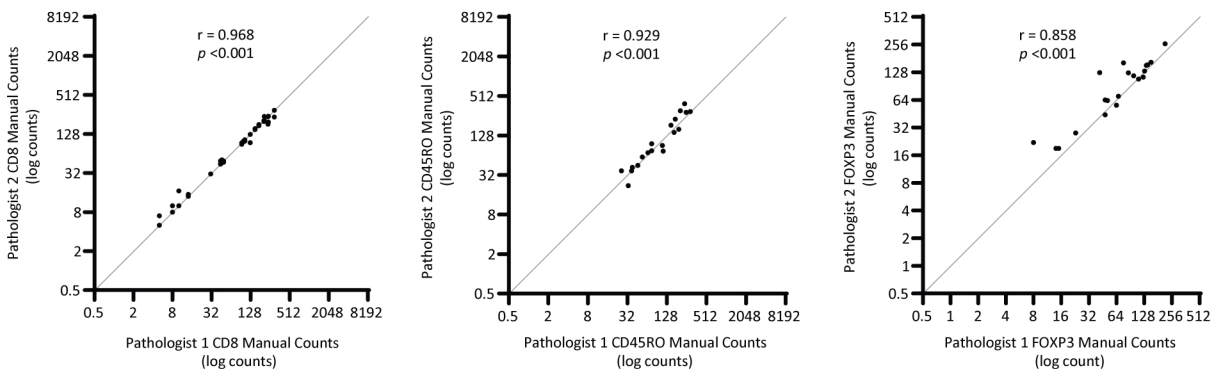
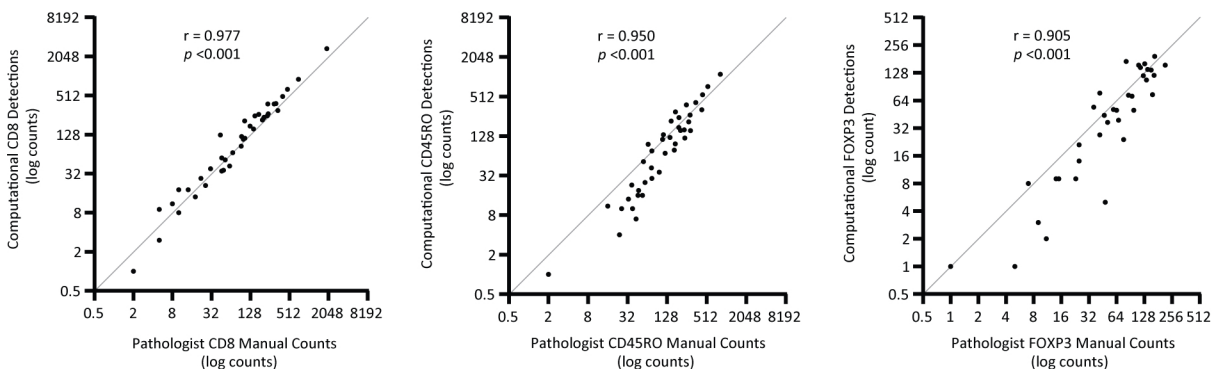


Figure 2

A Discovery Cohort



B Discovery Cohort



C Validation Cohort

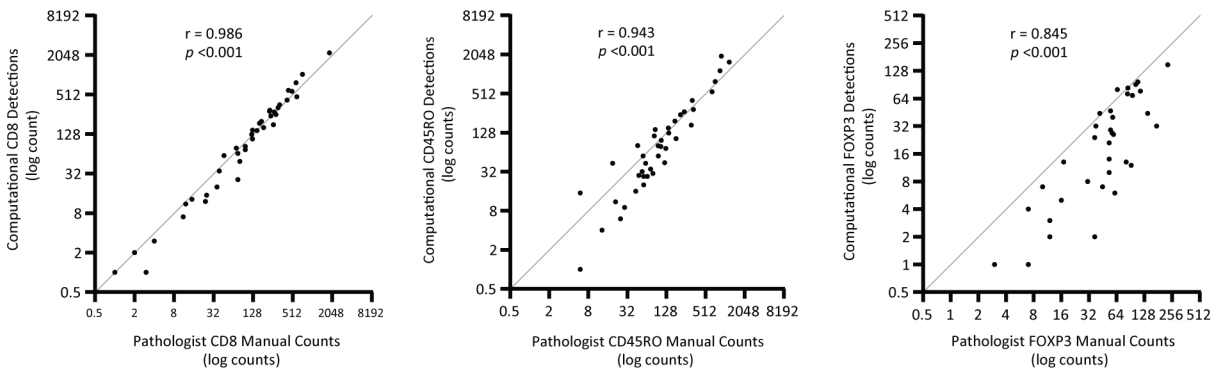
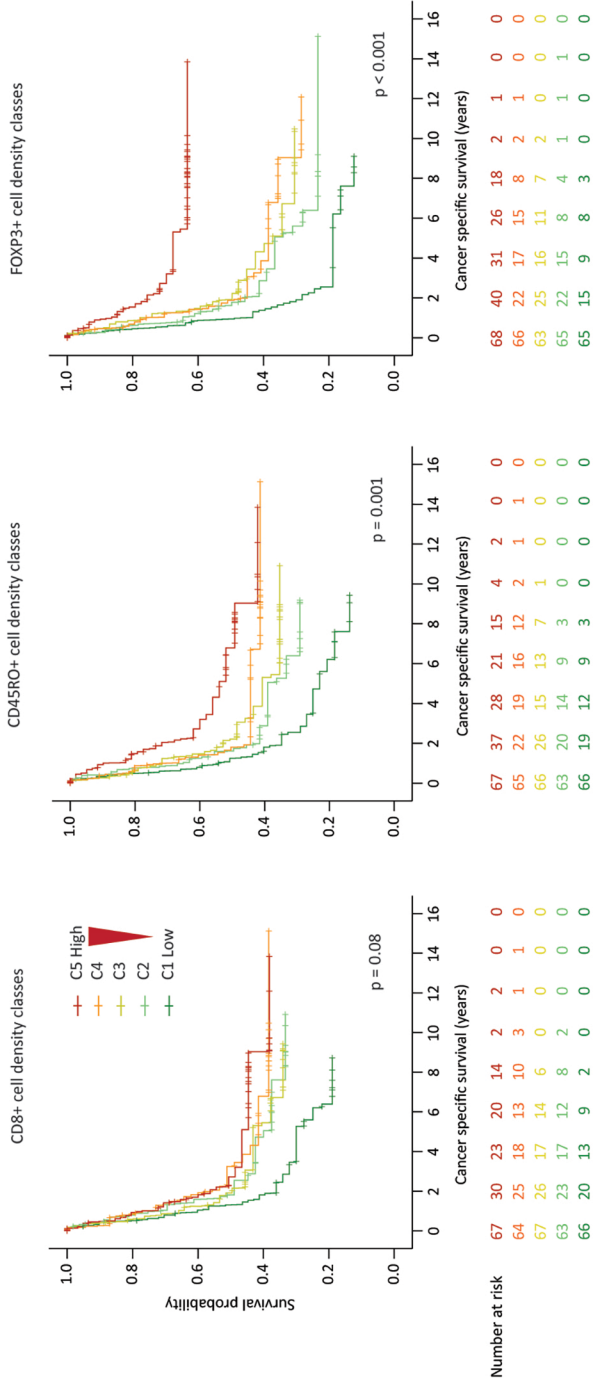


Figure 3

A



B

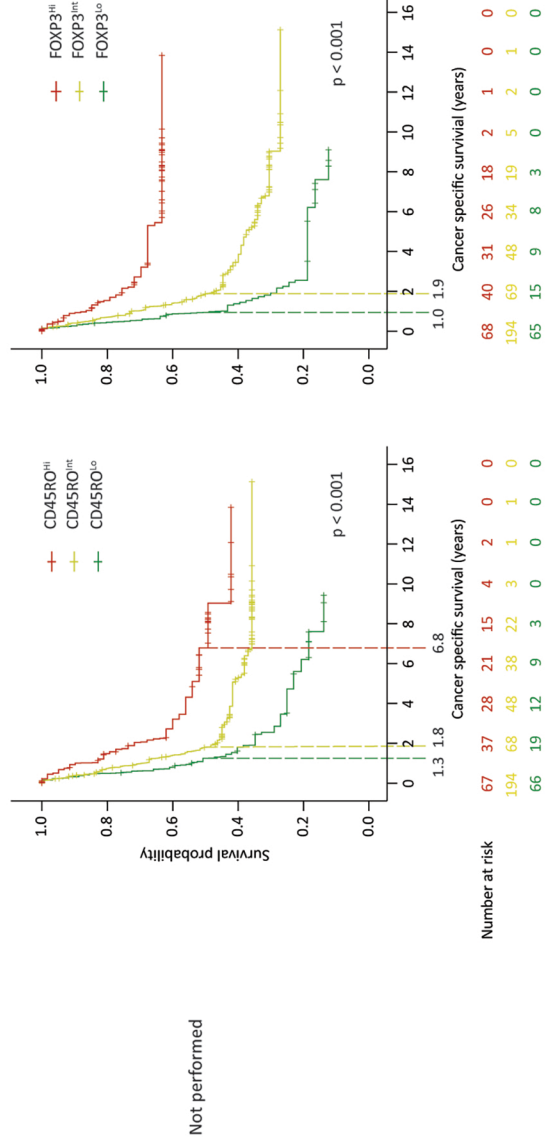
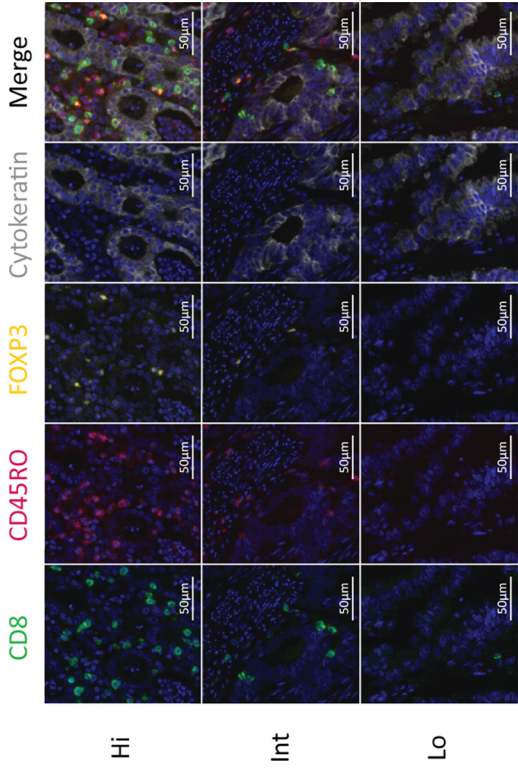
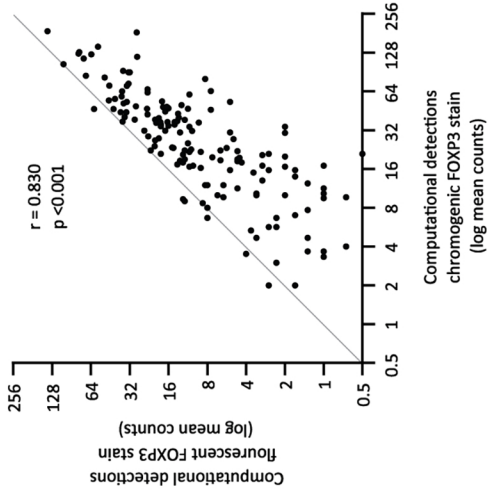


Figure 4

A



B



C

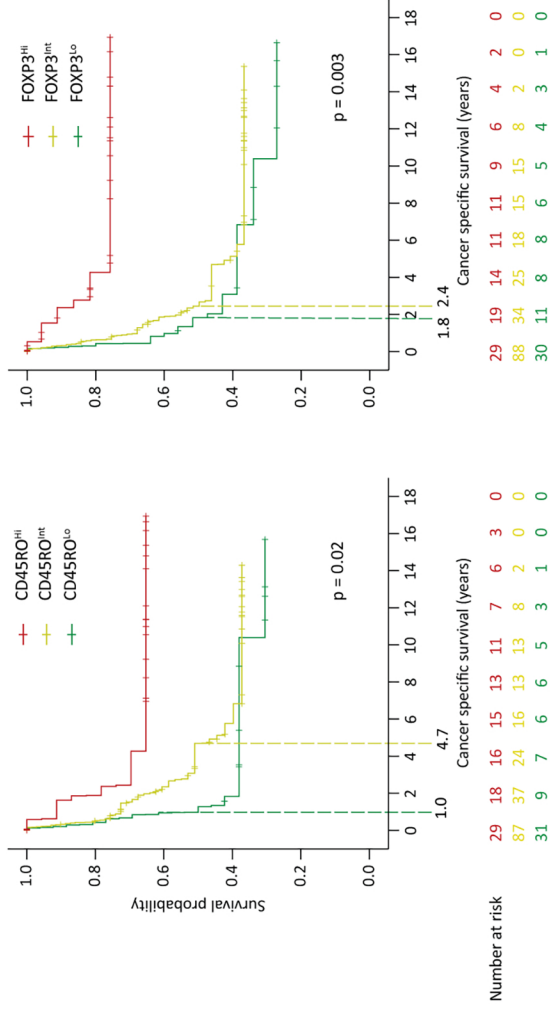
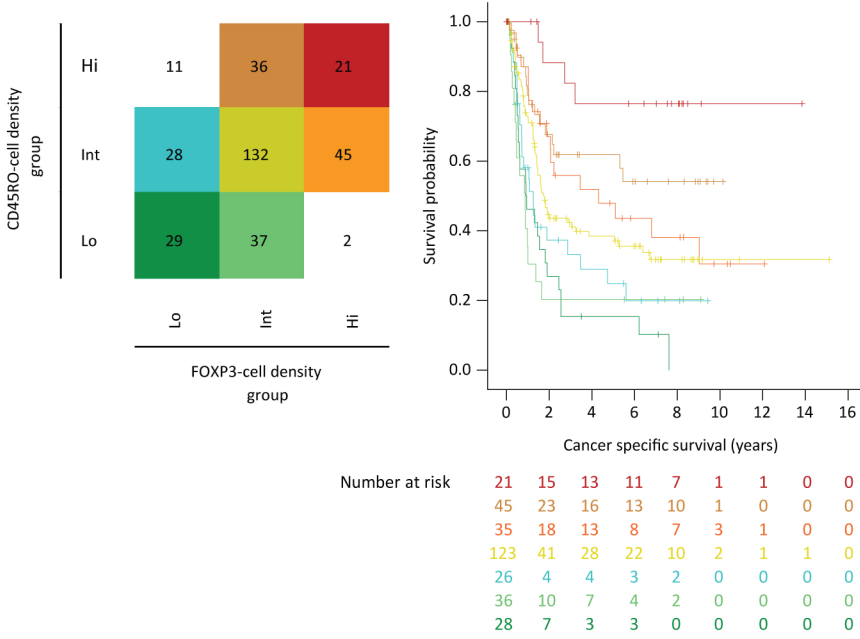
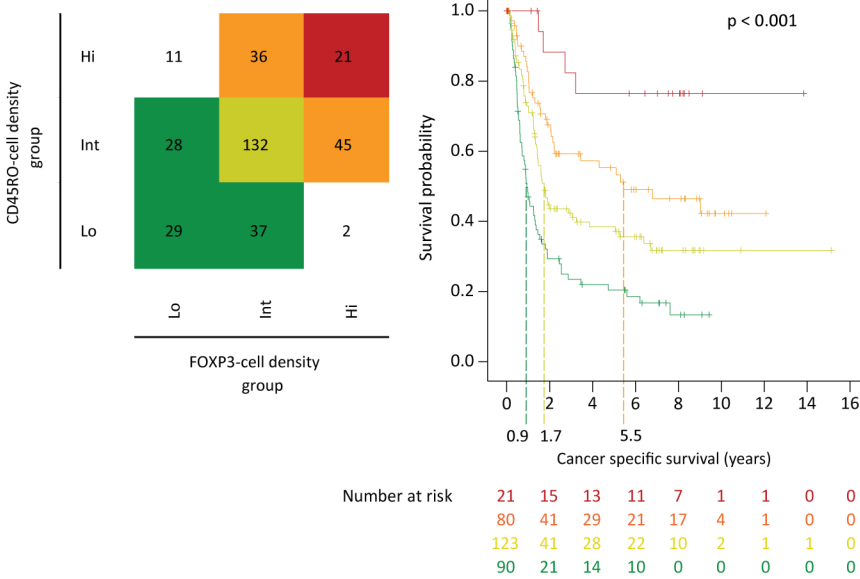


Figure 5

A Discovery Cohort

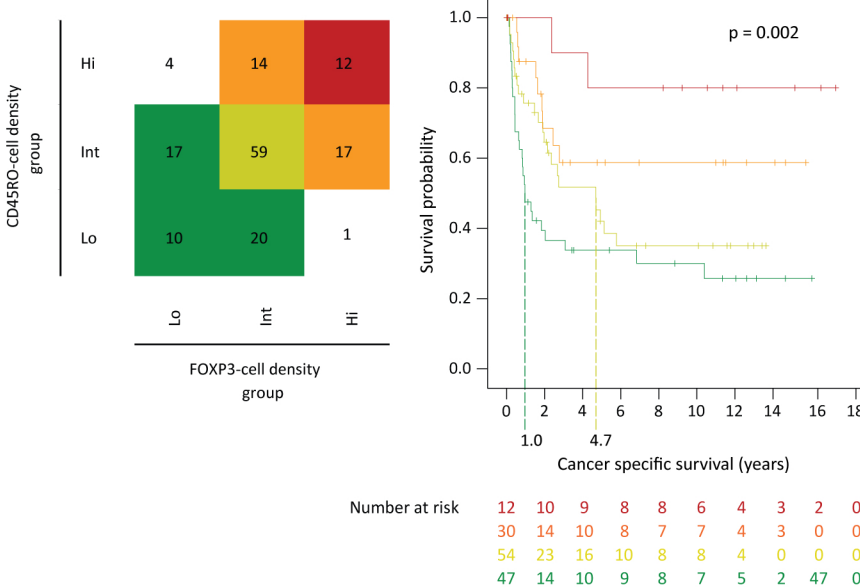


B Discovery Cohort



	EBV+	MMRd	MMRp EBV -
STIM4	50.0%	4.3%	5.2%
STIM3	37.5%	26.1%	25.7%
STIM2	12.5%	34.8%	40.3%
STIM1	0.0%	26.1%	25.0%

C Validation Cohort

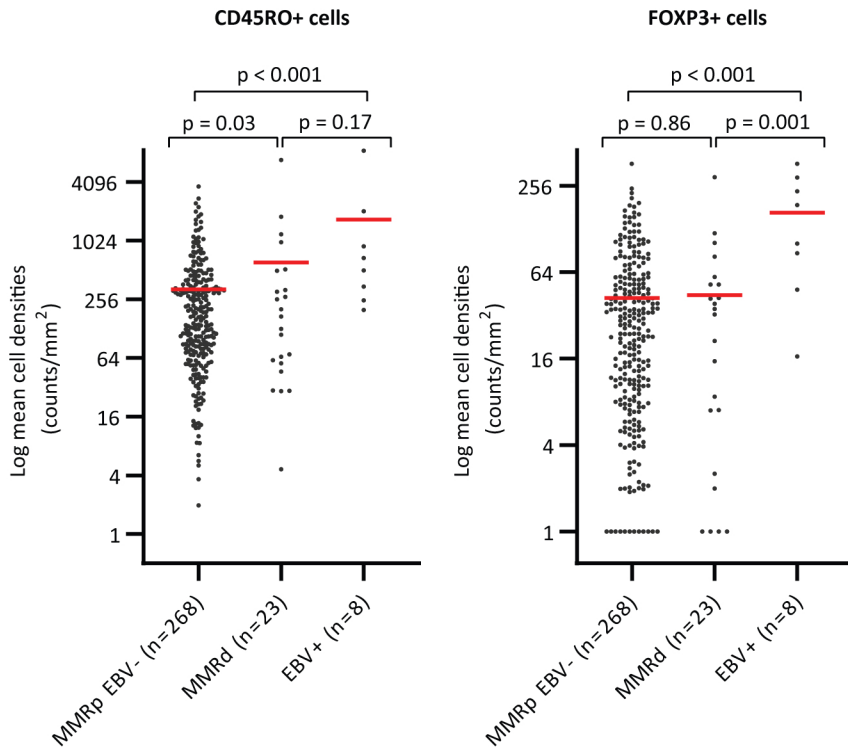


	EBV+	MMRd	MMRp EBV -
STIM4	8.3%	8.7%	7.6%
STIM3	41.7%	13.0%	18.6%
STIM2	41.7%	17.4%	42.2%
STIM1	0.0%	52.2%	29.7%

Figure 6

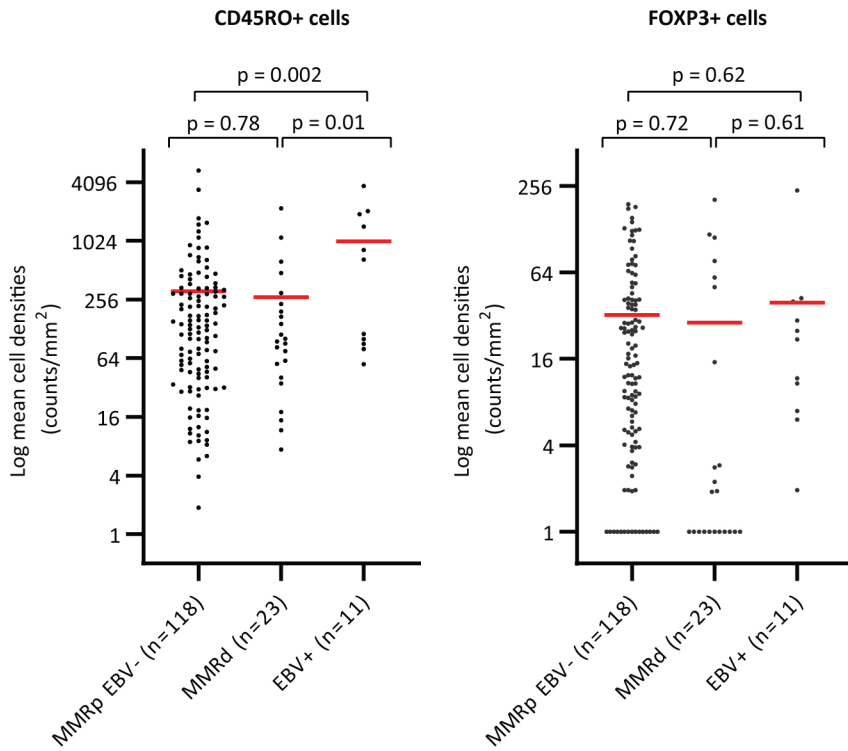
A

Discovery cohort



B

Validation cohort



Supplementary material

Computational image analysis of T-cell infiltrates in resectable gastric cancer: association with survival and molecular subtypes

B.R. Challoner, K. von Loga, A. Woolston, B. Griffiths, N. Sivamanoharan, M. Semiannikova,
A. Newey, L.J. Barber, D. Mansfield, L.C. Hewitt, Y. Saito, N. Davarzani, N. Starling,
A. Melcher, H.I. Grabsch and M. Gerlinger

Supplementary Table 1. Primary antibody and associated fluorophore application; supplier and dilution.

Primary antibody	Supplier	Dilution	Fluorophore (PerkinElmer)	Dilution
Anti-CD4	PerkinElmer	1:100	Opal 520	1:100
Anti-CD8	PerkinElmer	1:300	Opal 570	1:150
Anti-FoxP3	PerkinElmer	1:750	Opal 620	1:150
Anti-CD45RO	PerkinElmer	1:300	Opal 650	1:150
Anti-pan cytokeratin (AE1/AE3)	Dako	1:500	Opal 690	1:150

Supplementary Table 2. Vectra 3.0 scanning exposure times

Counterstain or primary antibody	Fluorophore	Filter	10x overview exposure time (ms)	20x scanning exposure time (ms)
Spectral DAPI	N/A	DAPI	5	40
Anti-CD4	Opal 520	FITC	40	150
Anti-CD8	Opal 570	Cy3	40	150
Anti-FoxP3	Opal 620	Texas Red	40	150
Anti-CD45RO	Opal 650	Cy5	40	150
Anti-pan cytokeratin (AE1/AE3)	Opal 690	Cy5	40	150

Supplementary Table 3. HALO algorithm setting for the nuclear, CD4-cell, CD8-cell, CD45RO-cell, FOXP3-cell and cytokeratin multicolour immunofluorescence computational detection.

	Setting
Analysis magnification	
Image zoom	1
Nuclear detection	
Nuclear contrast threshold	0.5
Minimum nuclear intensity	4
Nuclear segmentation aggressiveness	0.7
Fill nuclear holes	False
Nuclear size	9,700
Minimum nuclear roundness	0
Opal 520 (CD4) weight	0
Opal 570 (CD8) weight	0
Opal 620 (FOXP3) weight	1
Opal 670 (CD45RO) weight	0
Opal 690 (Pancytokeratin) weight	0
DAPI weight	1
Autofluorescence weight	0
Membrane and Cytoplasmic detection	
Maximum cytoplasmic radius	0.6
Membrane segmentation aggressiveness	N/A
Cell size	6,500
Opal 520 to Opal 690 membrane segmentation	False
DAPI membrane segmentation	False
Autofluorescence membrane segmentation	False
Opal 520 (CD4)	
Nucleus positive threshold	0.4
Cytoplasm positive threshold	0.3
Membrane positive threshold	7
Opal 570 (CD8)	
Nucleus positive threshold	1.4
Cytoplasm positive threshold	1.2
Membrane positive threshold	94
Opal 620 (FOXP3)	
Nucleus positive threshold	3
Cytoplasm positive threshold	89
Membrane positive threshold	89
Opal 670 (CD45RO)	
Nucleus positive threshold	1
Cytoplasm positive threshold	1
Membrane positive threshold	34
Opal 690 (Pan cytokeratin)	
Nucleus positive threshold	0.4
Cytoplasm positive threshold	1
Membrane positive threshold	21
DAPI	
Nucleus positive threshold	0
Cytoplasm positive threshold	70
Membrane positive threshold	70
Autofluorescence	
Nucleus positive threshold	26
Cytoplasm positive threshold	26
Membrane positive threshold	26

Supplementary Table 4. QuPath algorithm settings for chromogenic nuclear FOXP3 stain computational detection. 0 and 1+ detections were defined as FOXP3 negative, 2+ and 3+ detections were defined as FOXP3 positive.

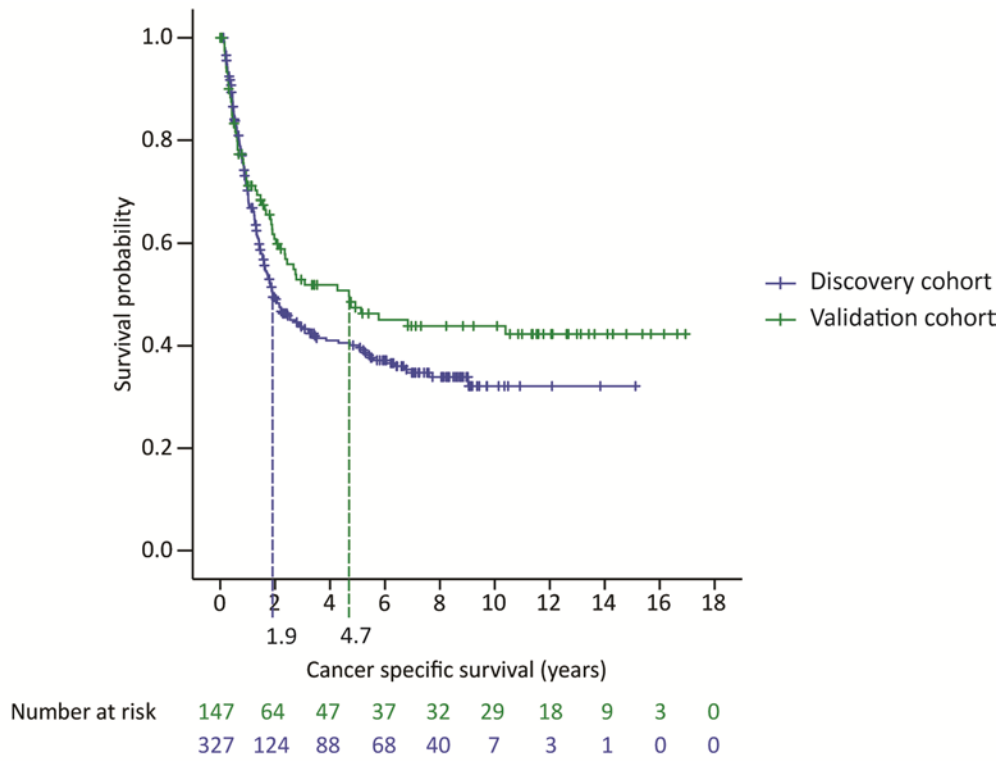
	Setting
Setup parameters	
Detection image	Optical density sum
Requested pixel size	0.5µm
Nucleus parameters	
Background radius	8.0µm
Median filter radius	0.0µm
Sigma	1.5µm
Minimum area	10.0µm ²
Maximum area	400.0µm ²
Threshold	0.1
Maximum background intensity	2.0
Split by shape	Checked
Exclude DAB (membrane staining)	Checked
Cell parameters	
Cell expansion	5µm
Include cell nucleus	Checked
General parameters	
Smooth boundaries	Checked
Make measurements	Checked
Intensity threshold parameters	
Score compartment	Nucleus: DAB OD mean
Threshold 1+	0.10
Threshold 2+	0.30
Threshold 3+	0.60
Single threshold	Unchecked

Supplementary Table 5. Multivariable Cox regression analysis with backwards Wald selection of non-significant variables within the discovery cohort.

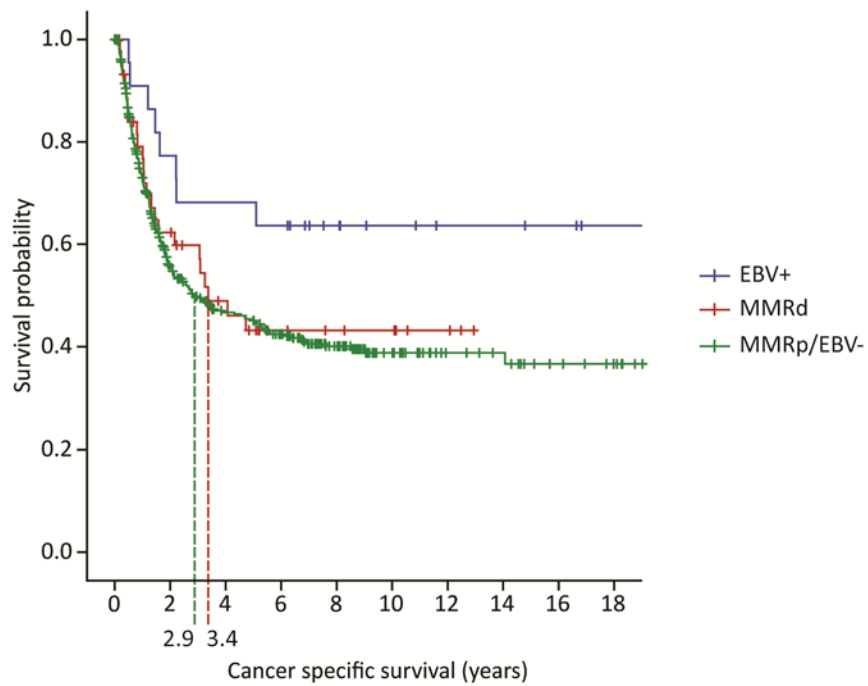
Variable	Initial analysis – Step 1			Step 2			Step 3			Final analysis – Step 4		
	Hazard ratio	(95% CI)	P value*	Hazard ratio	(95% CI)	P value*	Hazard ratio	(95% CI)	P value*	Hazard ratio	(95% CI)	P value*
	1.00	(Reference)	-	1.00	(Reference)	-	1.00	(Reference)	-	1.00	(Reference)	-
CD45RO-cell density												
Hi	1.70	(1.09 to 2.64)	0.02	1.69	(1.09 to 2.62)	0.02	1.72	(1.11 to 2.66)	0.02	1.71	(1.11 to 2.65)	0.02
Int	2.03	(1.21 to 3.41)	0.007	2.02	(1.21 to 3.39)	0.007	2.05	(1.23 to 3.42)	0.006	2.09	(1.25 to 3.48)	0.005
Lo	1.00	(Reference)	-	1.00	(Reference)	-	1.00	(Reference)	-	1.00	(Reference)	-
FOXP3-cell density												
Hi	2.02	(1.21 to 3.35)	0.007	2.00	(1.21 to 3.30)	0.007	1.98	(1.20 to 3.26)	0.007	2.00	(1.21 to 3.29)	0.007
Int	2.84	(1.55 to 5.22)	0.001	2.81	(1.55 to 5.12)	0.001	2.78	(1.53 to 5.05)	0.001	2.79	(1.54 to 5.08)	0.001
Lo	1.00	(Reference)	-	1.00	(Reference)	-	1.00	(Reference)	-	1.00	(Reference)	-
Stage (UICC TNM 7th Edition)												
pT3/4	0.21	(0.10 to 0.45)	<0.001	0.21	(0.10 to 0.45)	<0.001	0.21	(0.10 to 0.43)	<0.001	0.22	(0.10 to 0.45)	<0.001
pT1/2	1.00	(Reference)	-	1.00	(Reference)	-	1.00	(Reference)	-	1.00	(Reference)	-
pN1-3	0.47	(0.30 to 0.73)	0.001	0.47	(0.30 to 0.74)	0.001	0.47	(0.30 to 0.72)	0.001	0.45	(0.29 to 0.70)	<0.001
pN0	1.00	(Reference)	-	1.00	(Reference)	-	1.00	(Reference)	-	1.00	(Reference)	-
MIMR status												
MMRp	0.66	(0.35 to 1.22)	0.18	0.65	(0.35 to 1.22)	0.18	0.66	(0.36 to 1.23)	0.19	-	-	-
MMRd	1.00	(Reference)	-	1.00	(Reference)	-	1.00	(Reference)	-	1.00	(Reference)	-
Lauren classification												
Intestinal	0.84	(0.61 to 1.1)	0.29	0.84	(0.61 to 1.16)	0.28	-	-	-	-	-	-
Diffuse/Mixed	1.00	(Reference)	-	1.00	(Reference)	-	-	-	-	-	-	-
EBV status												
EBV-	1.13	(0.35 to 3.69)	0.84	-	-	-	-	-	-	-	-	-
EBV+	1.00	(Reference)	-	1.00	(Reference)	-	1.00	(Reference)	-	1.00	(Reference)	-

*Two-sided, Cox regression analysis.

Supplementary Figure 1. Cancer specific survival in the discovery and validation cohorts. Dashed lines indicate the median survival time for each cohort.



Supplementary Figure 2. Cancer specific survival in EBV+, MMRd and MMRp/EBV- groups across the discovery and validation cohorts combined. Dashed lines indicate the median survival time for each group, where this is reached.



Number at risk	24	17	15	14	9	6	4	4	3	1
	53	26	17	10	8	7	3	0	0	0
	456	197	145	122	84	41	21	18	11	7

Supplementary Figure 3. Median CD8-cell, CD45RO-cell and FOXP3-cell densities in the discovery and validation cohorts. Densities were off-set by 1 before log transformation. Red bars indicate the median and green whiskers the interquartile range.

